Use of boudinaged rigid objects as a strain gauge: Insights from analogue and numerical models

Nibir Mandal [a], Rajib Dhar [a], Santanu Misra [a], Chandan Chakraborty [b,*]

[a] *Department of Geological Sciences, Jadavpur University, Kolkata 700032, India*
[b] *Geological Studies Unit, Indian Statistical Institute, Kolkata 700108, India*

Abstract

Using analogue experiments we investigate how far the extensional strain estimated from an array of rigid boudins tracks the bulk extension of the host rock. The quadratic elongations of boudinaged objects (λ_b) were compared with the corresponding bulk quadratic elongations in physical models (λ_m) both for pure and simple shear. A noticeable difference occurs between the two, which depends on the aspect ratios of initial object (R_o) and boudins (R_b), boudin types, and the nature of bulk deformation. For a given R_o, the difference is proportional to R_b and tends to diminish with increasing R_o, when R_b is constant. The difference is normalized with the quadratic elongation measured from boudins (λ_b) to define a *departure factor* $\delta (= \overline{\lambda_m - \lambda_b}/\lambda_b)$. δ approaches a stable value with increasing λ_b. In pure shear the stable δ for torn symmetric boudins is larger ($>10^{-1}$) than that for asymmetric boudins, among which the planar type shows the departure close to 0. Boudins in pure shear show δ values smaller than that in simple shear. In case of simple shear, antithetic slip boudinage involves lower δ values compared to synthetic slip boudinage. Finite element models with elasto-viscous rheology also corroborate the experimental findings.
© 2007 Elsevier Ltd. All rights reserved.

Keywords: Boudinage; Slip sense; Quadratic elongation; Bulk extension; Pure shear and simple shear; Finite element model

1. Introduction

A line of work in structural geology develops new strain gauges (e.g. Ramsay, 1967; Gay, 1968; Mitra, 1976; Lisle, 1979; Bons and Jessell, 1995; Ramsay and Lisle, 2000; Hogan and Dunne, 2001; Treagus and Treagus, 2001; Lebit et al., 2005). Many rocks contain rigid objects of finite dimensions, e.g. elongate fossils, large mineral grains, layer-segments, that undergo brittle fragmentation into boudins during deformation (Ramberg, 1955). Boudins are potentially useful strain gauges and rheological indicators, but the issue exists as to how closely their deformation matches that of the host rock (Ramberg, 1955; Ghosh and Ramberg, 1976; Hossain, 1979; Ferguson, 1981, 1987; Lloyd and Ferguson, 1981; Burg and Harrris, 1982;

Mandal et al., 2000; Passchier, 2001; Passchier and Druguet, 2002; Lloyd and Condliffe, 2003; Treagus and Lan, 2004).

Theory and experiments show that boudinage within a ductile matrix may occur either by tensile and/or shear fracturing (e.g. Ramsay and Huber, 1983; Jordan, 1991; Ji and Zhao, 1993; Mandal et al., 1994, 2001). The initial fracture mechanism and development control subsequent boudin geometry (Ghosh and Ramberg, 1976; Mandal and Khan, 1991; Hanmer and Passchier, 1991; Passchier and Druguet, 2002; Goscombe and Passchier, 2003; Goscombe et al., 2004). A recent classification of boudins (Goscombe et al., 2004) considers both their initial geometry and kinematic behavior (Fig. 1). This classification forms the framework for our analysis, as we consider the effectiveness of boudins as strain gagues for the case of torn boudins, and both synthetically and antithetically slipped dilational and planar boudins.

As strain gauges, torn symmetric boudins can be restored to the initial object length to determine finite extension, assuming

---

* Corresponding author.
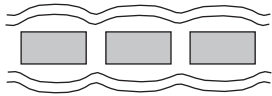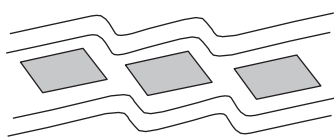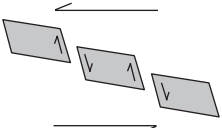*E-mail address:* chandan@isical.ac.in (C. Chakraborty).
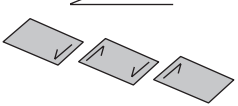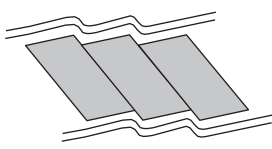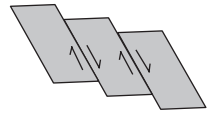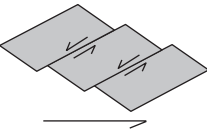
Fig. 1. Types of boudins (after Goscombe et al., 2004) considered for the analysis.

Fig. 2. Schematic sketches of set-up for experimental boudinage under (a) pure shear; and (b) simple shear. Scale bar: 3 cm.
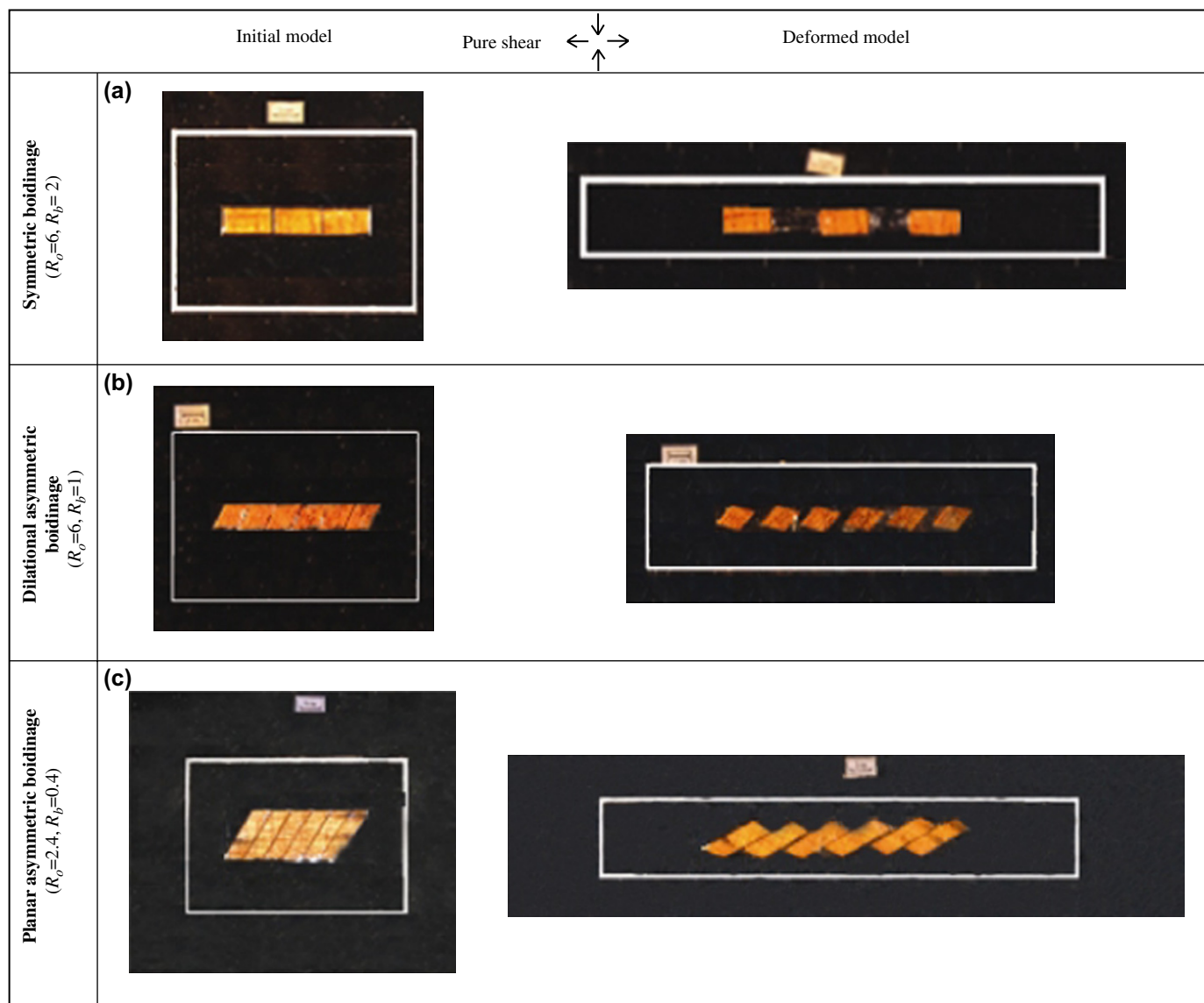
Fig. 3. Boudinage structures in experimental models deformed in pure shear: (a) symmetric; (b) dilational asymmetric; and (c) planar asymmetric types. White shade: wooden boudins, black shade: pitch (matrix). Rectangular boxes indicate the magnitude of bulk strain. Objects were initially oriented along the principal extension direction. Scale bar: 1 cm.

little or no internal deformation of boudins (Ramsay, 1967; Beach, 1979; Ferguson, 1981; Ramsay and Huber, 1983; Ghosh, 1993). Asymmetric boudins may yield finite strains from their rotation (Ramsay and Huber, 1987; Nur and Ron, 1987; Karmakar and Mandal, 1989; Ghosh, 1993). The purpose o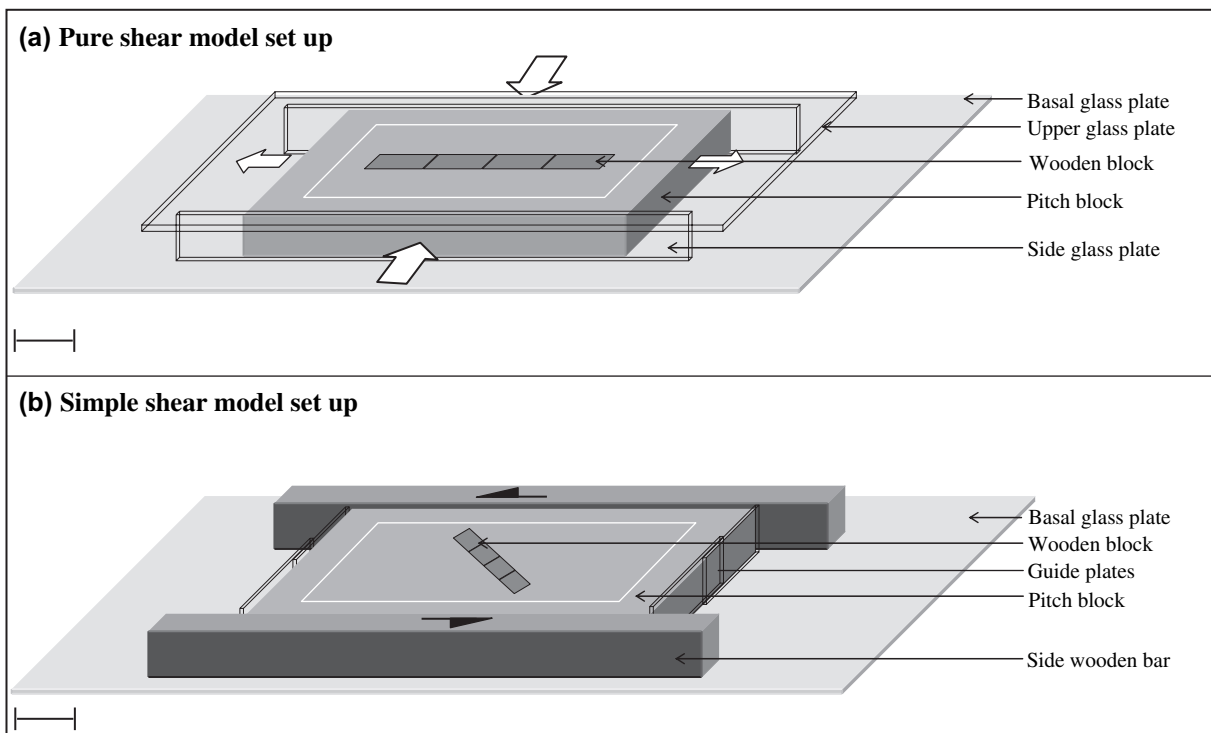f this paper is to assess accuracy of the finite strain estimated from a row of rigid boudins for determining the two-dimensional finite strain of the host rock. We estimate the similarity from analogue and finite-element simulations for both simple and pure shear type of bulk deformation. The difference in extensional strains of a boudinaged object and the host rock tends to vanish only when the objects are infinitely extended across the boudin axis. However, in case of objects with finite length the difference is likely to become stable at a finite stage of deformation, which can be utilized to improve the accuracy of bulk strain estimation.

2. Analogue experiments

Analogue physical experiments were performed with models containing a rigid object (wood) placed within a pitch block (21 cm × 16 cm × 4.5 cm) (cf. Mandal and Khan, 1991). The wooden object was 1.5 cm thick, but its length and width were varied between 6−10 cm and 1−2.5 cm, respectively. Boudins were created by cutting the wooden strip in pieces with straight cuts that were oriented at 45° or 90°. The segmented wooden strip was then placed within the pitch block with the entire thickness inside the pitch so that its surface remained at the level of the pitch block. The interfaces between the rigid object and matrix were adherent, allowing no slip during the deformation. The pitch was visco-elastic, but mainly behaved as a viscous material at room temperature (30 °C) and slow strain rates (in the order of 10^{-6}/s). Its viscosity was about 5×10^5 Pa s.
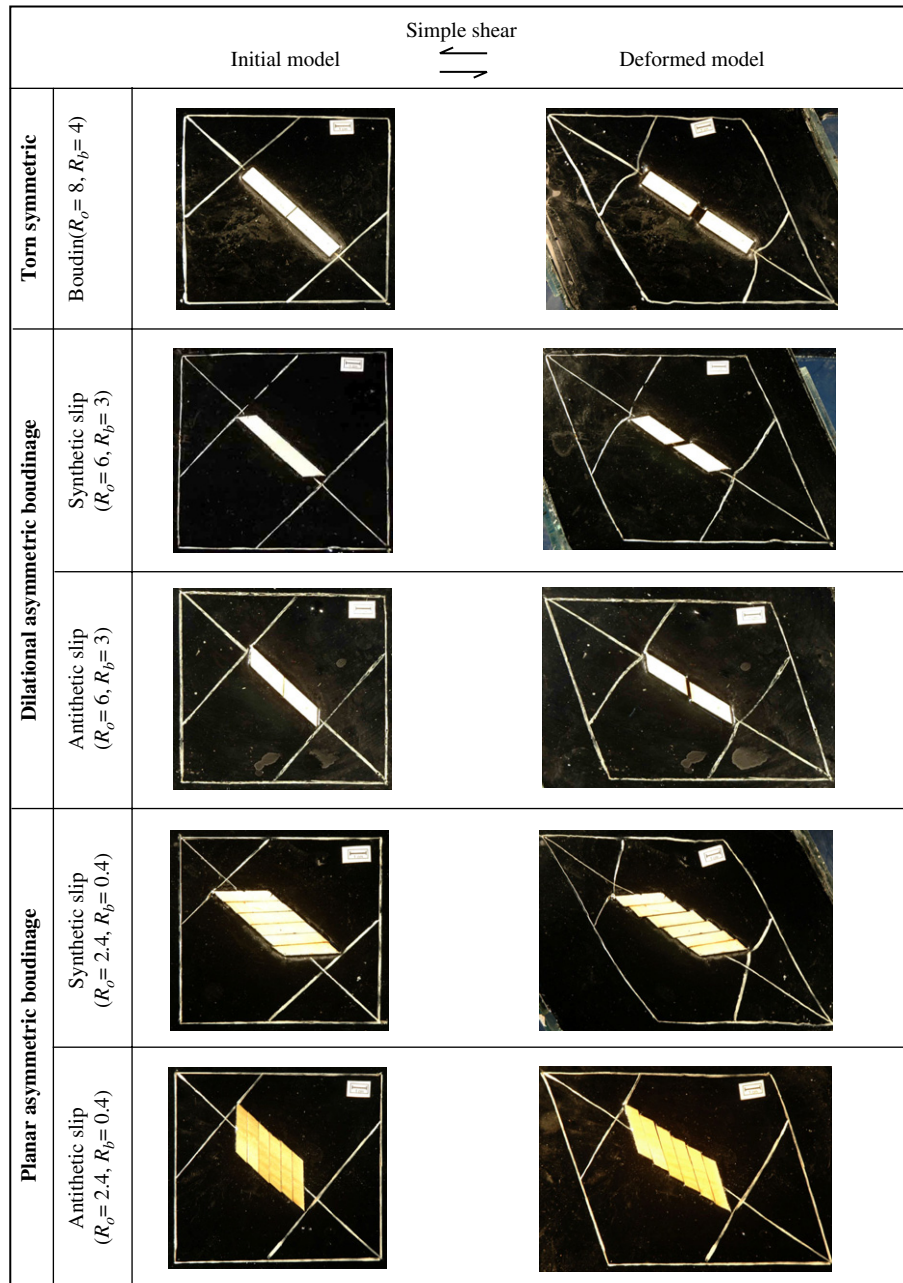
Fig. 4. Boudinage structures in experimental models deformed in sinistral simple shear. Scale bar: 1 cm.

Models were placed on a horizontal (0.5 cm thick) glass plate with a film of commercial liquid soap to minimize model to plate friction (Fig. 2). Models were deformed by pure shear or simple shear on a hydraulically controlled horizontal platform, containing two moving parallel rigid bars. For pure shear experiments, the rigid bars were driven horizontally toward each other at equal velocities. The model surface was covered with a horizontal glass plate to inhibit the material flow in the vertical direction, resulting in bulk extension in the orthogonal horizontal direction. We placed two vertical glass plates, covering the model thickness, in between the model and the driving bars, and lubricated their surfaces with liquid soap for smooth flow

of pitch in the horizontal direction (Fig. 2a). For simple shear, two wooden plates with rough surfaces were placed so that the pitch remained firmly stuck to the plates. Models were sheared by moving the two hydraulic bars in the parallel directions (Fig. 2b). The lateral faces of model were confined with two parallel, guiding plates that also moved with the parallel bars.

In our experiments we dealt with three types of boudins (Fig. 1): (1) torn-symmetric; (2) dilational asymmetric; and (3) planar asymmetric in both pure shear and simple shear (Fig. 2). To develop no-slip boudinage structures in pure shear, the initial cuts were made at a right angle to the long dimension
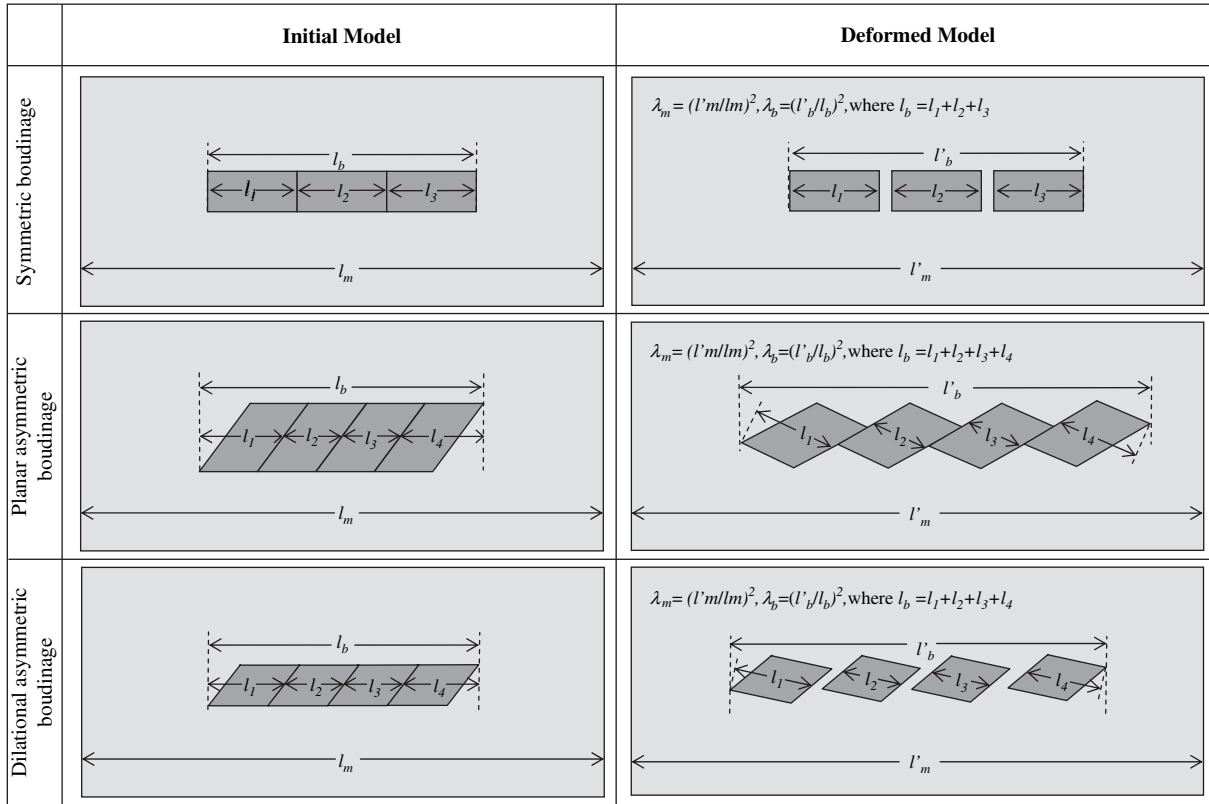
Fig. 5. Calculations of quadratic elongation (λ) for the three types of boudinage structure. λ_m: bulk quadratic elongation of model, λ_b: quadratic elongation of boudinaged objects (see text for details).

3. Strain analysis

3.1. Approach

During an experiment, the length of a boudin array was measured at successive stages of progressive deformation. The finite quadratic elongation of object was determined, say λ_b, for finite bulk extension of model, λ_m (cf. Ferguson, 1981) as in the following equations:

$$\lambda_b = \left(\frac{l'_b}{l_b}\right)^2 \text{ and } \lambda_m = \left(\frac{l'_m}{l_m}\right)^2 \qquad (1a, b)$$

where $l_b = l_1 + l_2 + l_3 + l_4 + \ldots\ldots$.

l_b is the initial length of segmented object, where l_1, l_2,.. are the lengths of individual segments. l_b' is the length of object following boudinage. l_m is the initial distance between two points far away from the object measured in the direction of boudinaged object and l_m' is distance between the two points following deformation (Fig. 5). l_b and l_m for any segment of a boudinage structure are likely to change at different rates, as reflected from the drag of a set of marker lines drawn across the objects in experiments (Fig. 6).

To study the difference we prepared a graph in $\lambda_b - \lambda_m$ space. λ_b versus λ_m variation would be represented by a straight line with $\lambda_b = \lambda_m$, if the stretching objects track the bulk extension in the model. $\lambda_b - \lambda_m$ plots indicate that

of rectangular objects at an equal spacing, and the object was oriented along the principal direction of bulk extension. During pure shear, the rectangular segments were separated simultaneously from one another, forming torn symmetric boudins (Fig. 3a). To simulate dilational and planar asymmetric structures in pure shear, the cuts were oriented at an angle of 45° to the long dimension of object (Fig. 3b,c). Dilation rather than planar slip dominated the kinematic behavior of boudins with asymmetric faces for pure shear when the face spacing exceeded half of the boudin thickness. For simple shear, boudinage was simulated for the case where the line of boudins occurred at 45° to the shear zone boundary and verging into the shear direction (Fig. 4). Objects with cuts initially either orthogonal or at an angle of 45° to their long dimension (verging in the shear direction) gave rise to synthetic-slip boudinage (Fig. 4). To simulate antithetic-slip boudinage oblique cuts were at an angle of 45° verging against the shear direction (Fig. 4; cf. Passchier and Druguet, 2002; Goscombe et al., 2004).

Following Ramsay's (1967) method, we measured the extensional strain by length balancing of separated boudins (Fig. 5) at successive stages of model deformation, which will be described as *boudinage strain*. For planar and dilational asymmetric boudins, the boudinage strain was determined by measuring the distance between the opposite edges of boudinaged object in the bulk extension direction, and comparing it to the initial line length.

Fig. 6. Successive stages of model deformation in pure shear experiments showing distortion patterns of lines perpendicular to the bulk extension direction (horizontal). Scale bar: 1 cm.

the object strain does not follow the bulk extension at any stage of deformation. The deflection from the $\lambda_b = \lambda_m$ line can be described by a factor:

$$\delta = \frac{\lambda_m - \lambda_b}{\lambda_b} \tag{2}$$

Using Eq. (2) a precise value of the actual extensional strain in deformed rock can be obtained if the value of δ is known.

Experimental investigations reveal that λ_b versus λ_m variations and the corresponding δ value, are functions of three factors: (1) aspect ratio of object (R_o); (2) aspect ratio of boudins (R_b); and (3) the type of boudinage, which may all be identified in natural systems. In this study R_o and R_b are length parallel to layering versus thickness ratios of object and individual boudins respectively on a section perpendicular to the boudin axis (Ghosh, 1993).

(a)

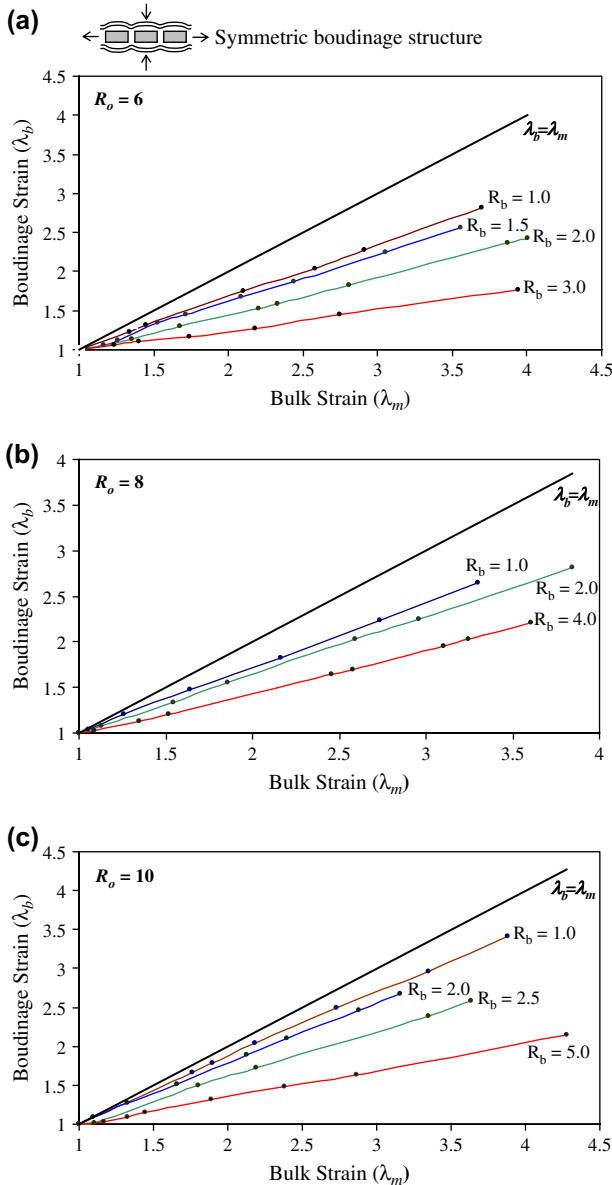Symmetric boudinage structure

(b)

(c)

Fig. 7. Plots of (symmetric) boudinage strain (λ_b) versus bulk model strain (λ_m) from physical experiments for pure shear. Initial aspect ratio $R_o = 6, 8, 10$ in (a), (b) and (c), respectively. R_b: Boudin aspect ratio. Solid lines show $\lambda_b = \lambda_m$.

3.2. Analysis with torn symmetric boudins

In experimental symmetric boudinage λ_b varies with λ_m, maintaining a consistent difference from the $\lambda_b = \lambda_m$ line (Fig. 7). The difference is larger for larger boudin aspect ratio R_b (Fig. 7a), whereas it becomes small with increasing object aspect ratio R_o (Fig. 7b,c). Calculated departure factor δ varies positively with λ_b, but has a tendency to attain a stable value (Fig. 8). At small R_b (e.g. 1), the stable value is attained along a gentle gradient after a large boudinage strain. On the other hand, when R_b is large (say 3) the variation becomes steeper, but there is a tendency of δ to approach a stable value at relatively lower boudinage strain. The stable value of δ is directly proportional to R_b, but inversely related to R_o (Fig. 8a–c, Table 1a). Evidently, boudinage in infinitely extended layers

(comparable to objects with $R_o = \infty$) are thus likely to track the bulk extension perfectly, and thereby show $\delta = 0$.

In simple shear, torn-symmetric boudins developed only when the aspect ratios of both boudins and object were large (≥ 4 and 8 respectively), and the cuts were at right angle to the long axis of object (Fig. 4). They had stretching behaviour similar to that in pure shear. However, the departure factor δ in simple shear is relatively high, and appears to have a larger stable value (~ 0.7, Fig. 8d, Table 1b).

3.3. Analysis with dilational asymmetric boudins

Dilational asymmetric boudins show $\lambda_b - \lambda_m$ variations as a function of boudin aspect ratio, similar to those for symmetrical boudins (Fig. 9a). However, the estimated extensional strain maintains relatively lower differences with the bulk strain, as reflected from smaller stable values of δ, e.g. 0.2 when $R_b = 1$ (Fig. 9b). With increasing R_b δ becomes large, however remaining less than that of symmetrical boudins (Figs. 8a and 9b, Table 1a).

In simple shear experiments objects, with aspect ratios less than 8 produced asymmetric boudins. For $R_o = 6$, rectangular boudins ($R_b < 4$) underwent rotation and displacement, giving rise to dilational asymmetric boudinage with synthetic slip. The δ values of these structures are large (>0.5, Fig. 10a), as compared to asymmetrical boudins in pure shear (0.15, Fig. 9b, Table 1). The shape of boudins also influences the δ factor (Fig. 10a,b). For example, when $R_o = 6$ and $R_b = 2$, the stable value of δ appears to be nearly 1 for rectangular shape, which decreases close to 0.7 when the shape becomes rhombic. The sense of slip is an additional factor in determining δ, where antithetic slip boudinage involves lower departures relative to that with synthetic slip (Fig. 10b, Table 1b).

3.4. Analysis with planar asymmetric boudins

In pure shear, the estimated extension differed little with the actual extension in model. With decrease in R_b, this difference is further reduced (Fig. 11a). Their departure factor δ approached a stable value, as in the other two types of boudinage (Fig. 11b). However, this is very low (<0.1), for example $\delta = 0.03$ for $R_b = 0.4$ (Table 1a).

In simple shear, antithetic slip boudinage better tracks the bulk extension ($\delta < 0.2$, Fig. 11c) in respect to synthetic slip boudinage ($\delta > 0.5$, Fig. 11c, Table 1b). Furthermore, the two types show contrasting relations between δ and R_b. δ is directly proportional to R_b when inter-boudin slip is antithetic, whereas the relation is inverse in case of synthetic slip. It may be noticed that planar boudinage with both synthetic and antithetic slip involves δ larger than that in pure shear (Table 1a,b).

4. Boudinage in finite element models

4.1. Modelling approach

We simulated boudinage structures in two-dimensional finite-element models (Lloyd and Ferguson, 1981; Ramsay

Symmetric boudinage
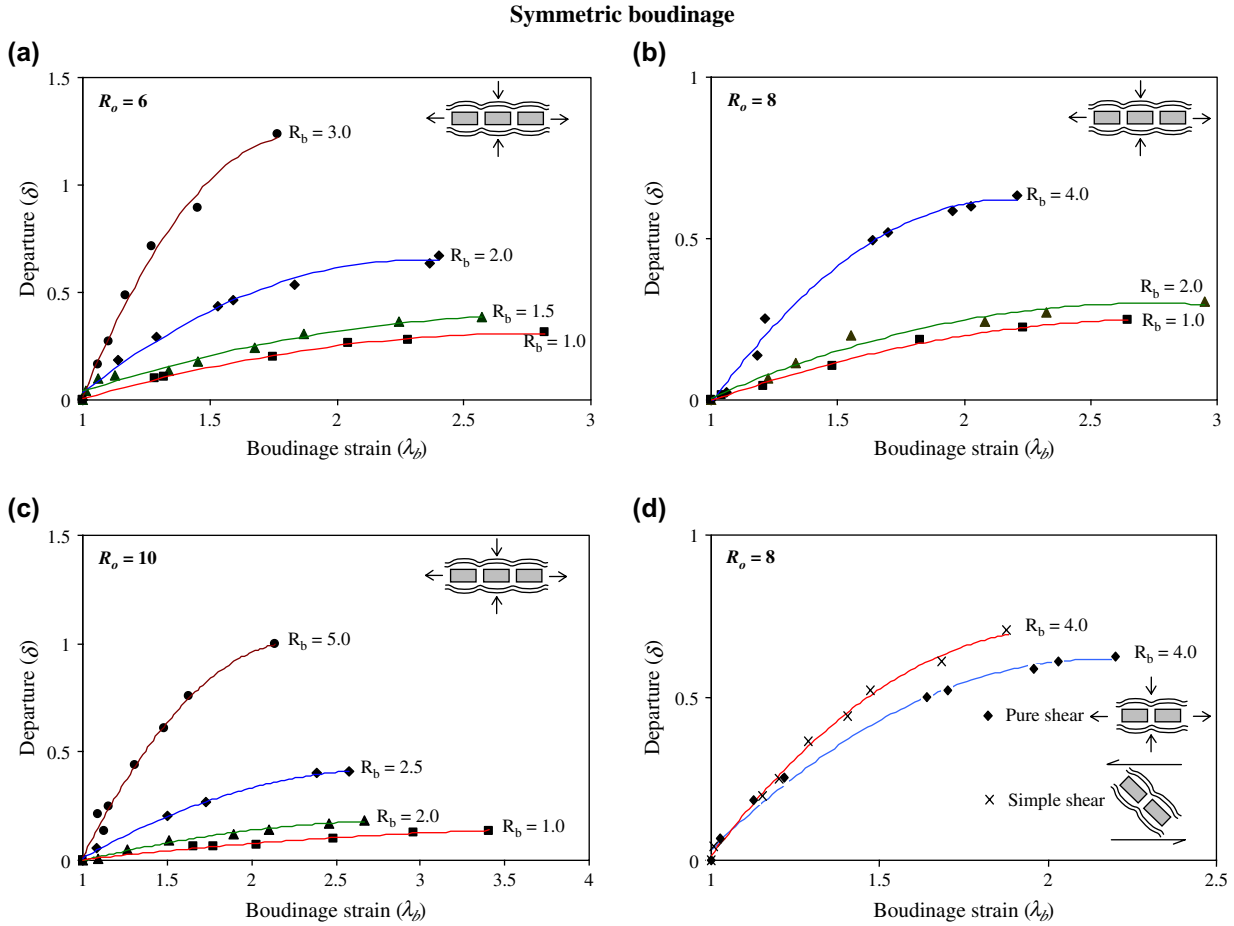
Fig. 8. Plots of the departure factor δ for different aspect ratios of boudins. (a) $R_o = 6$; (b) $R_o = 8$; (c) $R_o = 10$. (d) Plot showing δ versus λ_b variation for pure and simple shear type of bulk deformation. R_o: Initial aspect ratio of object, R_b: Boudin aspect ratio.

Fig. 9. (a) Variation of boudinage strain (λ_b) with bulk model strain (λ_m) for asymmetric dilational boudins in pure shear experiments; and (b) plots of the corresponding departure factor δ with λ_b.

Table 1
Summary of experimental data

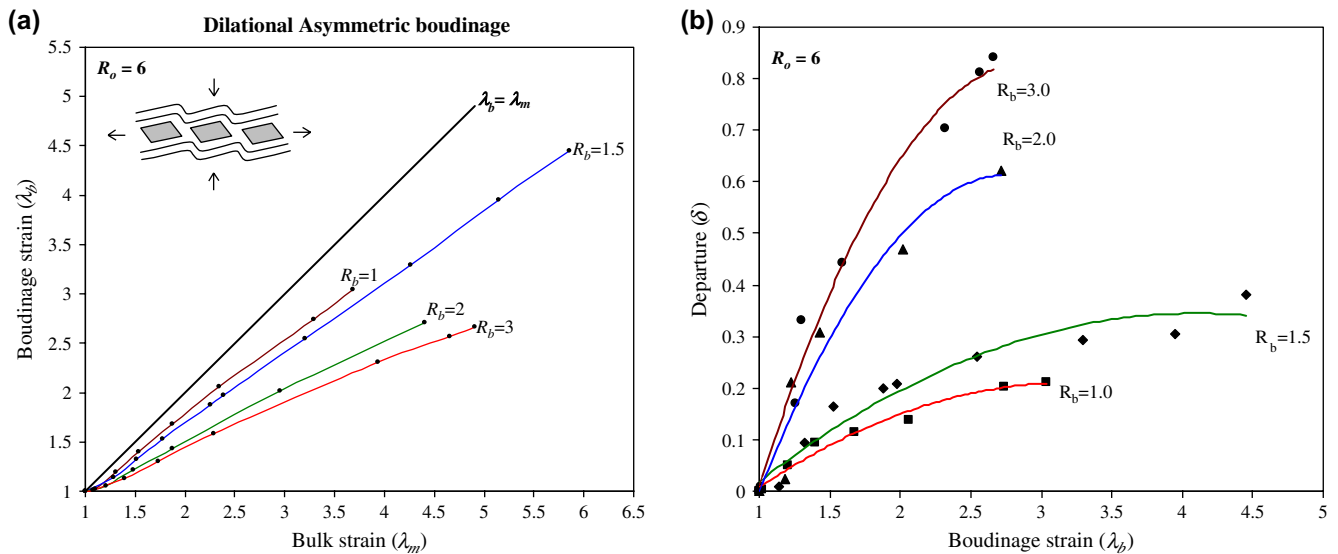| Boudin types			R_o	R_b	Stable δ value
(a) Pure shear					
Torn symmetric			6	1	0.31
				1.5	0.38
				2	0.64
				3	~1.23
			8	1	0.24
				2	0.36
				4	~0.63
			10	1	0.13
				2	0.18
				2.5	0.41
				5	~0.99
Dilational asymmetric			6	1	0.21
				1.5	0.32
				2	0.62
				3	0.84
Planar asymmetric			2.4	0.4	0.09
				0.5	0.04
(b) Simple shear					
Boudin types			R_o	R_b	Stable δ value
Torn symmetric			8	4	~0.7
Dilational asymmetric	Synthetic slip	Rectangular	6	1	~0.58
				2	~1
				3	~1.2
		Rhombic	6	1	0.35
				2	~0.63
				3	~1.01
	Antithetic slip		6	1	0.23
				2	0.56
				3	0.98
Planar asymmetric	Synthetic slip		2.4	0.4	0.67
				0.5	0.56
	Antithetic slip		2.4	0.4	0.19
				0.5	0.26

~ indicates approximate stable values of δ.

Fig. 10. Variation of departure factor δ with boudinage strain (λ_b) for dilational asymmetric boudins of: (a) rectangular; and (b) rhombic shapes. Note that synthetic slip boudinage (solid line) involves larger differences in extensional strain compared to that of antithetic slip (dash line).

and Lisle, 2000; Treagus and Lan, 2004). Visco-elastic rheology with the following constitutive equation was considered in the modeling (cf. Passchier and Druguet, 2002).

$$\frac{d\epsilon}{dt} = \frac{1}{2\mu}\frac{d\sigma}{dt} + \frac{\sigma}{2\eta}, \qquad (3)$$

where ϵ and σ are the instantaneous strain and stress respectively, and μ and η are the Maxwell shear modulus and viscosity respectively. The finite element models were developed using ANSYS (version 9.0) software. Employing the operation mode in structural mechanics of this software, we modeled symmetrical and planar asymmetric type boudins in the following manner. We took a rectangular region (*Region 2*) with length and width dimensions several times that of the boudinage object (Fig. 12), described as *Region 1* in the foregoing description. *Region 1* was then segmented by taking a number of narrow zones (*Region 3*) to form boudins. A model therefore consists of three regions: *Region 1* (boudin), *Region 2* (matrix) and *Region 3* (inter-boudin space) (cf. Passchier and Druguet, 2002).
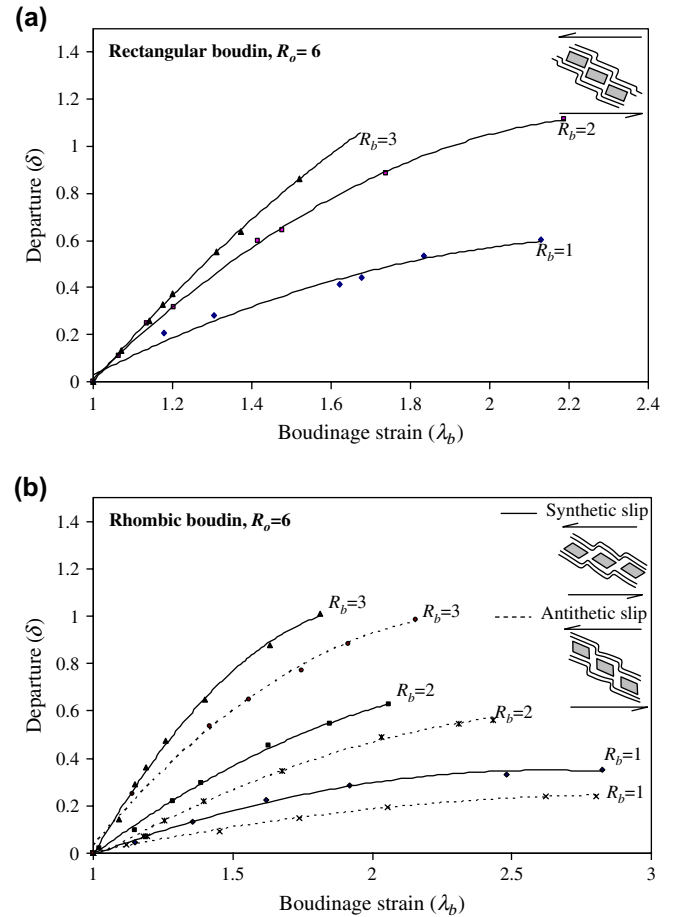
Implementation of the constitutive relation (Eq. (3)) in the finite element code requires inputs of the bulk modulus of materials in addition to shear modulus and viscosity (cf. Passchier and Druguet, 2002). The bulk modulus of a region has been calculated utilizing the shear modulus and the Poisson's ratio (Table 2). The viscosity of *Region 1* was chosen 500 times that of *Region 2* so that the boudins would not undergo large internal deformation in the flowing matrix (*Region 2*). *Region 3* was assigned with a low viscosity, simulating separation zones in the boudinaged layer. We employed the technique of free mesh generation in finite element models (Fig. 13), where the mesh concentration was different in the three different regions (Table 2). Models were deformed either in pure shear or simple shear. During the deformation, boudins did not remain strictly rigid, as in the physical experiments.

To achieve the necessary deviatoric stress for generating a pure shearing deformation, we applied compressive and tensile stresses of equal magnitude at the model boundaries (Fig. 12). Model dimensions were taken much larger than that of objects to achieve nearly a homogeneous strain at the model boundaries. The sides of the model were 32 times the width of object. It was verified that for this model dimension
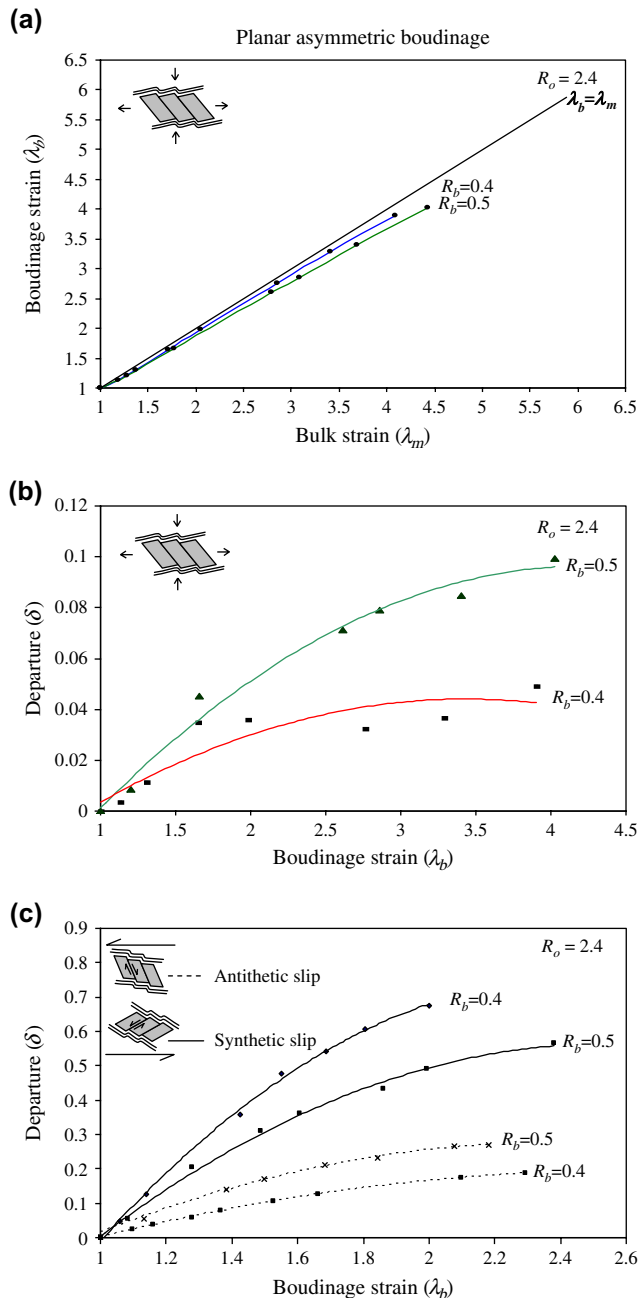
(a)

Planar asymmetric boudinage

(b)

(c)

Fig. 11. (a) Boudinage strain (λ_b) versus bulk strain (λ_m); and (b) δ versus boudinage strain (λ_b) for planar asymmetric boudins in pure shear. (c) Plots showing the influence of inter boudin slip on the departure factor δ in simple shear. Note that boudinage with synthetic slip involves larger difference with the bulk strain relative to that with antithetic slip.

the boundaries of model remained virtually straight for a finite bulk quadratic strain less than 3, and the overall change in the model shape was close to that of pure shear. Bulk finite strain in the model was increased in successive steps at constant stresses at the model boundaries. Simple shear experiments in finite element models were performed employing shear displacements at the four boundaries of models. The run time was set to achieve strain rates in the range of 10^{-7}/s (Table 2). At each step, the nodal displacements at the boundaries of *Region 1* and *Region 2* were obtained from model runs, and a relation

between the bulk extension in the model and that in the boudinaged object was determined.

4.2. Model results

For pure shear, the variation of λ_b with λ_m deviates from the $\lambda_m = \lambda_b$ line, indicating that the boudins record less extension than the host (Fig. 14a). This difference is larger for large aspect ratios of boudins, as with the analogue experiments. On the other hand, the variation for planar asymmetric boudinage show relatively little departures from the $\lambda_m = \lambda_b$ line. Finite element models thus indicate that the extensional strain determined from asymmetric boudins will be close to the bulk strain, as revealed from physical experiments. We estimated the departure factors for both symmetric and planar asymmetric structures as a function of λ_b. δ values tend to assume a stable value with increasing λ_b, and are approximately consistent with the experimental data (Fig. 14b,c). However, physical models show slightly lower δ values. This difference is probably due to differences in the configurations of physical and finite element models. In case of physical model, the objects had a three-dimensional geometry, which is considered in two dimensions in case of finite element models. Moreover, inter-boudin spaces in finite element models were completely filled with a material, which in case of physical models were gaps, partly filled by the matrix material.

Finite element models run in simple shear show that planar asymmetric boudinage with antithetic slip maintains lower differences from the actual bulk strain, as observed in physical model experiments (Fig. 15a). The value of the departure factor δ is much smaller compared to that involving synthetic slip, which approximately follows our experimental findings (Fig. 15b).

In summary, finite element models reveal that planar asymmetric boudinage tracks the bulk extension more closely compared to symmetric boudinage, as observed in physical models. Secondly, the departure factor for given boudin geometry tends to assume a stable value, which approximately matches with that of physical models.

5. Discussion

5.1. Practical use of boudinaged objects in strain analysis

Boudinaged objects, such as fossils, large mineral grains and clasts in deformed rocks can be used for determination of extensional strain (Ramsay, 1967). Previous studies as well as our experimental results show that boudinaged objects of finite length do not exactly track the bulk extensional strain. Ramsay and Huber (1983) have described boudinaged structures of elongate amphibole crystals hosted in mica schist containing recrystallized quartz grains (Fig. 6.13B, p. 101, Ramsay and Huber, 1983). The quartz grains are strongly flattened defining a prominent fabric. The dominant aspect ratio of flattened quartz grains is estimated about two. Assuming their initial shape to be equant, the ratio can be taken as a measure of
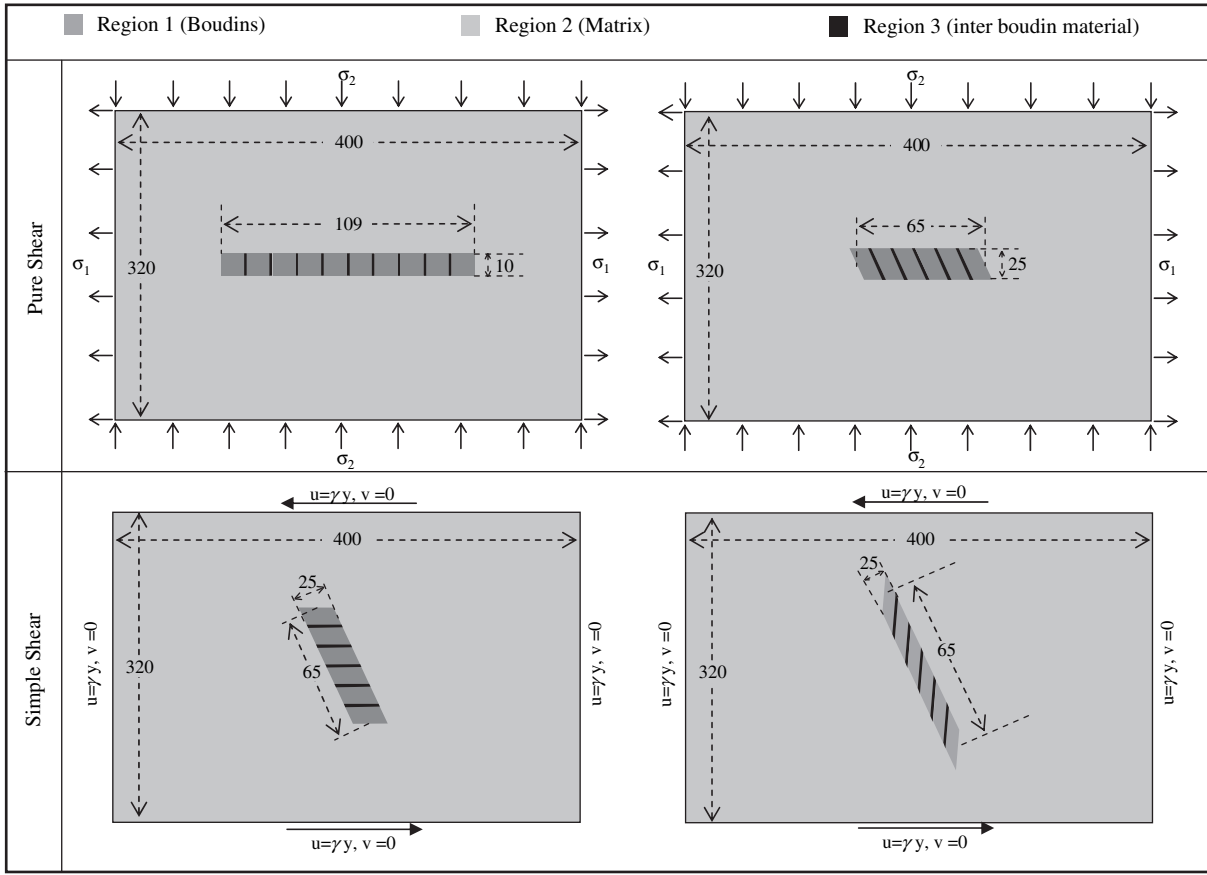
Fig. 12. Model parameters and boundary conditions used for finite element modeling of boudinage structure in pure and simple shear.

bulk strain in the bulk medium. Considering a plane strain condition, the bulk quadratic elongation thus appears in the order of 2. Extension obtained from displaced amphibole boudins is estimated to be 1.2. The departure factor δ is thus 0.65, which is large and comparable to that observed in our pure shear experiments. However, natural boudins show somewhat higher values of δ compared to that shown by experimental ones of similar geometry. This difference may result from factors such as bulk deformation condition, non-synchronous development of fractures in amphibole crystals, etc. To analyze the departure factor for simple shear we used boudinage structures of granite mylonites from a brittle-ductile shear zone in the Peninsular Gneiss, south India (Fig. 16). The mylonites contain boudinaged feldspar pophyroclasts in a plastically deformed quartz-rich matrix. We estimated extensional strains from

boudinaged feldspar grains, and compared it with that obtained from the flattened shapes of recrystallized quartz grains. Boudinaged porphyroclasts always show a difference between boudinage strain and the actual bulk extension, as observed in physical experiments. The departure factor estimated for nearly symmetrical boudins is 0.74 when the object and the boudin aspect ratios are 1.28 and 0.66 respectively (Fig. 16a). Dilational asymmetric structures (Fig. 16b; average $R_b = 1.08$ and $R_o = 2.18$) with synthetic slip show δ factor in the order of 0.45. The initial aspect ratio of the structures is lower than those simulated in physical experiments. However, the departure factor is consistent with the trend of variation obtained from experimental runs for different R_o values. Dilational asymmetric boudins (Fig. 16c; $R_o \approx 5$, $R_b \approx 2.6$) show departure factor δ = 1.06. It may be noted that the order of the

Table 2
Physical parameters considered in finite element modeling

Material properties	Regions	Bulk Modulus (kPa)	Shear Modulus (kPa)	Viscosity (kPa s)	Density (kg/m³)
	Region 1 (Boudin)	2×10^8	1.2×10^8	5×10^{18}	3×10^6
	Region 2 (Matrix)	2×10^7	1.2×10^7	9.996×10^{15}	3×10^6
	Region 3 (Inter boudin material)	2×10^6	1.2×10^6	9.996×10^{15}	3×10^6
Mesh type	Free Mesh (Numbers- Region 1: $19-22 \times 10^2$, Region 2: $8-14 \times 10^3$, Region 3: $3-8 \times 10^2$)				
Boundary condition	Bulk deformation	Pressure (kPa)	Displacement (m)	Time (s)	Stain rate (s⁻¹)
	Pure shear	2×10^5	−	8×10^8	3.5×10^{-7}
	Simple shear (Sinistral)	−	$u = \gamma y, v = 0$	8×10^8	3.5×10^{-7}

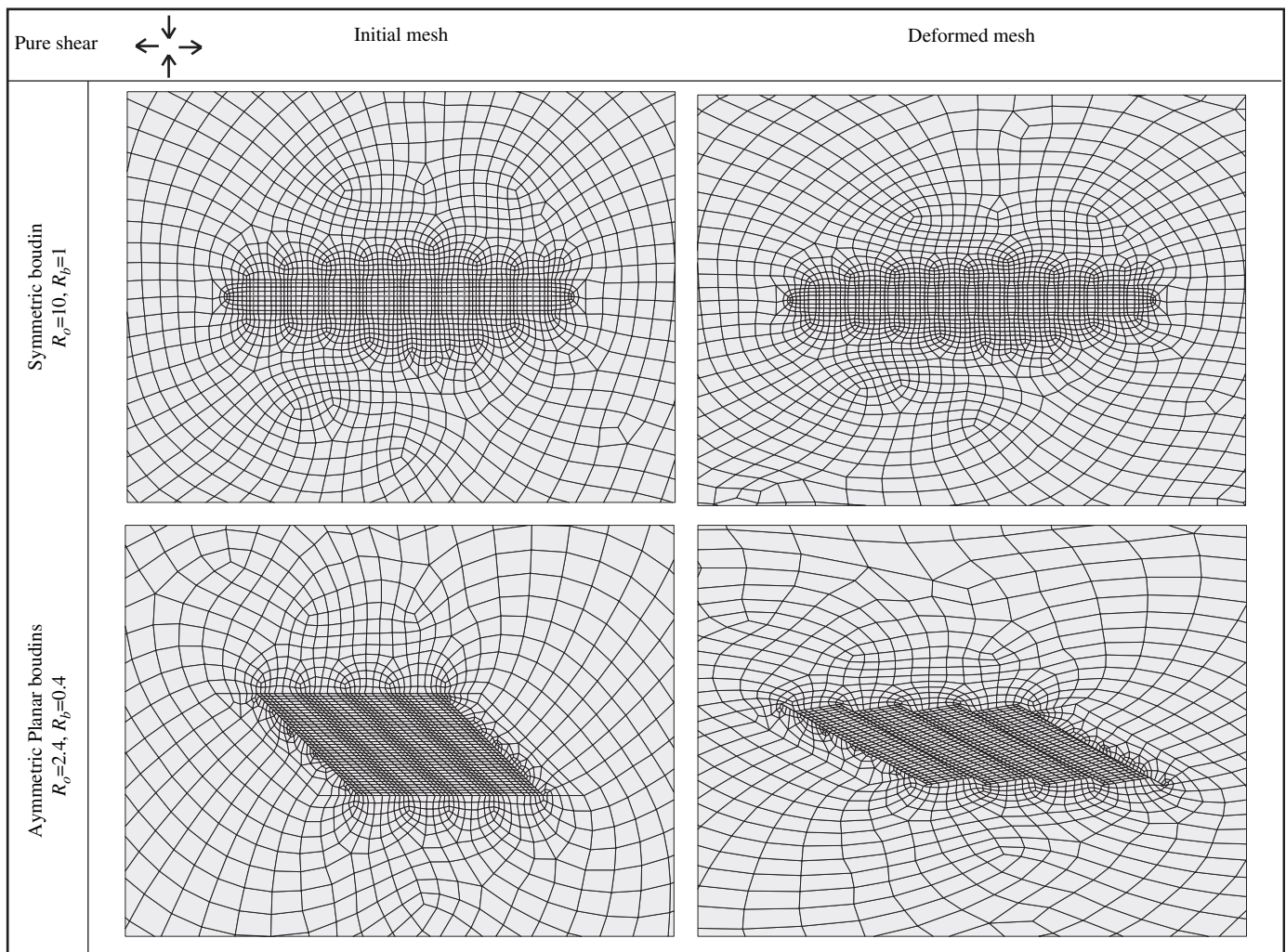| Pure shear ←↓→ ↑	Initial mesh	Deformed mesh
Symmetric boudin $R_o=10, R_b=1$		
Asymmetric Planar boudins $R_o=2.4, R_b=0.4$		

Fig. 13. Close views of finite element models showing initial objects and corresponding symmetric (upper) and planar asymmetric (lower) boudinage structures in pure shear.

departure factor is consistent with that of boudins of similar geometry in physical experiments under simple shear (Fig. 10a).

These examples support the contention that boudinage strain underestimates bulk strain. We gave an effort to refine the strain gauge by quantifying the difference as a function of geometrical and kinematic parameters. We cite an example below to address this issue. Ramsay and Huber (1983) present a strain analysis using quadratic elongations of differently oriented boudinaged belemnites. The aspect ratios of initial belemnites (Section 6.4, Fig. 6.8 of Ramsay and Huber, 1983) are estimated in the range of 7 to 10, whereas those of individual boudins fall in the range of 1.25 to 1.45. According to our analysis, the stable value of the departure factor δ corresponding to this boudin geometry would be around 0.2 for both pure and simple shear types of bulk deformation. The departure value is small, and the extensional strains determined from belemnites are therefore close to the actual bulk strain. However, a more precise value of the finite quadratic elongations could be obtained considering the departure factor in the following equation: $\lambda_m = (1 + \delta) \lambda_b$. It follows from the experimental results that quadratic elongation measured from

belemnites will lead to a better approximation of the bulk extension if they are multiplied by a factor 1.2.

5.2. Limitations in experiments

In our experiments the objects were placed on the surface of pitch slabs, keeping their third dimension (i.e. the dimension along boudin axis) inside pitch. This dimension was about 0.5 times the initial thickness of object. The third dimension of object was constant in all the experiments, and the experiments attempted to show influence of the length to thickness ratio of object in the difference between boudinage strain and the actual bulk extension. In our study it has not been shown how the three-dimensional shape can influence the departure factor δ. To generalize the value of δ for different types of boudins we need to advance the experimental study considering a range of 3D shapes of objects.

Based on different experimental runs, our study intends to show that δ factor will attain a stable value with increasing boudinage strain (λ_b). However, in some of the experiments, especially with large boudin aspect ratios (R_b), λ_b required

(a)

(b)

(c)

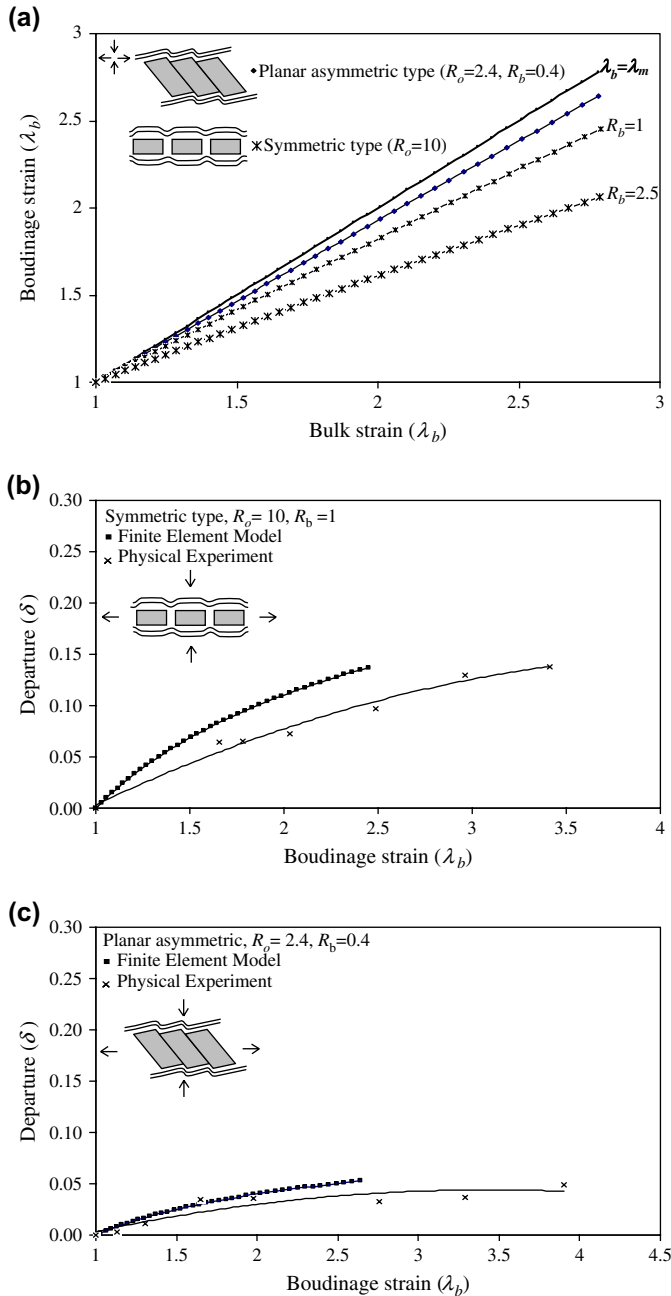Fig. 14. Calculated plots of data obtained from finite element models in pure shear. (a) Boudinage strain (λ_b) versus bulk strain (λ_m). Departure factor δ versus boudinage strain (λ_b) for (b) symmetric; and (c) planar asymmetric boudins. In (b) and (c) data obtained from physical experiments are shown for comparison.
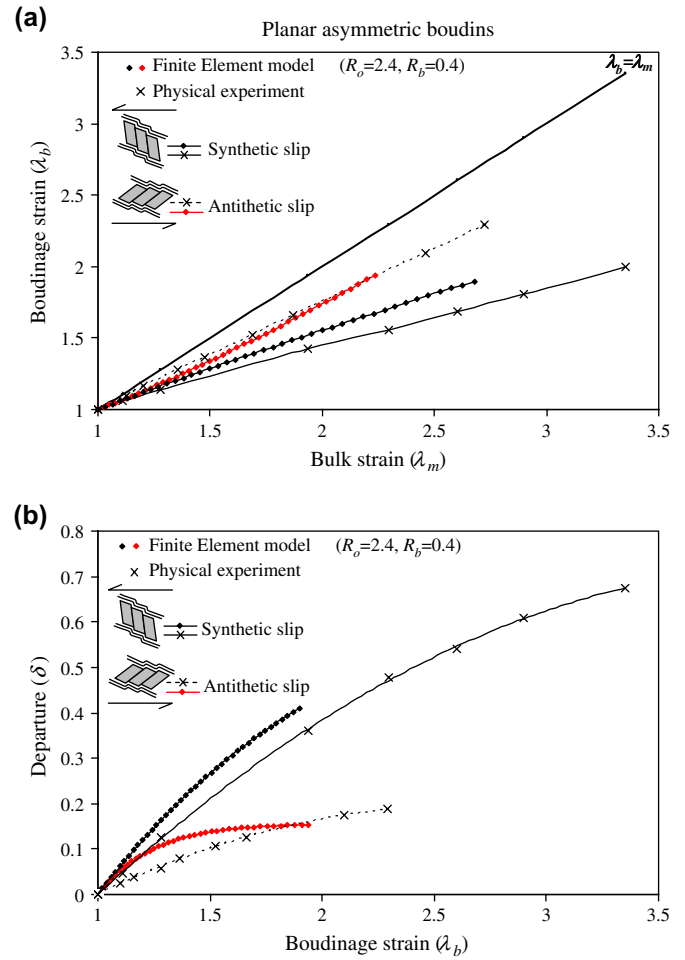

(a)

(b)

Fig. 15. Calculated plots of data obtained from finite element models and physical experiments, simulating planar asymmetric boudinage with synthetic and antithetic slip in simple shear. (a) Boudinage strain (λ_b) versus bulk strain (λ_m). (b) Departure factor δ versus boudinage strain (λ_b).

direction. Secondly, this method is convenient for fieldwork, as the edges of objects in geological situations may be irregular and the boudins may not be perfectly arranged along a straight line. In case of asymmetric type boudins, we determined the departure factor considering the lengths along the central line, and compared with that obtained from the maximum length technique. The difference estimated considering the length in these two methods always remains small (Fig. 17). We preferred the maximum length technique as it involves lower values of the departure factor δ.

6. Conclusions

(1) Extensional strain determined from boudinage structures is less than the actual bulk strain, and the difference is a function of initial aspect ratio of boudinaged objects, aspect ratio of boudins and the type of boudinage. The difference tends to attain a stable value with increasing boudinage strain. The stable value is larger for larger boudin aspect ratio, whereas it has an inverse relation with initial object aspect ratio.
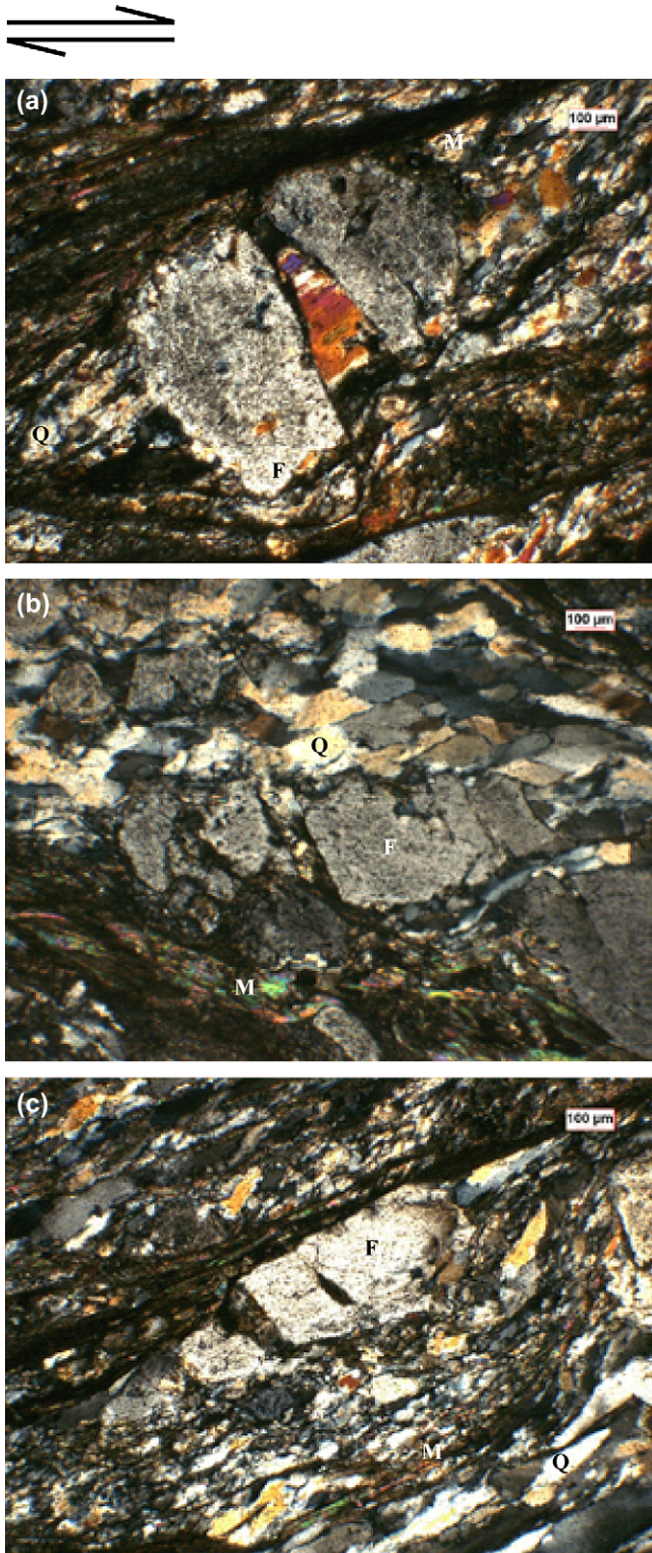
for reaching the stable values were not achieved, as the runs were stopped at large model deformations (e.g. $\lambda_m > 4-5$). It may be noted that, for a given λ_m the boudinage strain (λ_b) drops with increasing R_b. The experimental data in these cases thus demonstrate approximate stable values of δ, as indicated in Table 1.

We measured the initial length of object by taking the distance between two extreme end points of the object along the length dimension. The method was employed to account the maximum length occupied by the object along the extension

Fig. 16. Granite mylonites showing boudinaged feldspar porphyroclsts (**F**) within a matrix of recrystallized quartz grains (**Q**) and mica (**M**). Scale bar = 100 μm.

(2) Torn symmetric type of boudins shows the largest difference between boudinage strain and the actual bulk extension, whereas the planar asymmetric type involves the lowest difference.
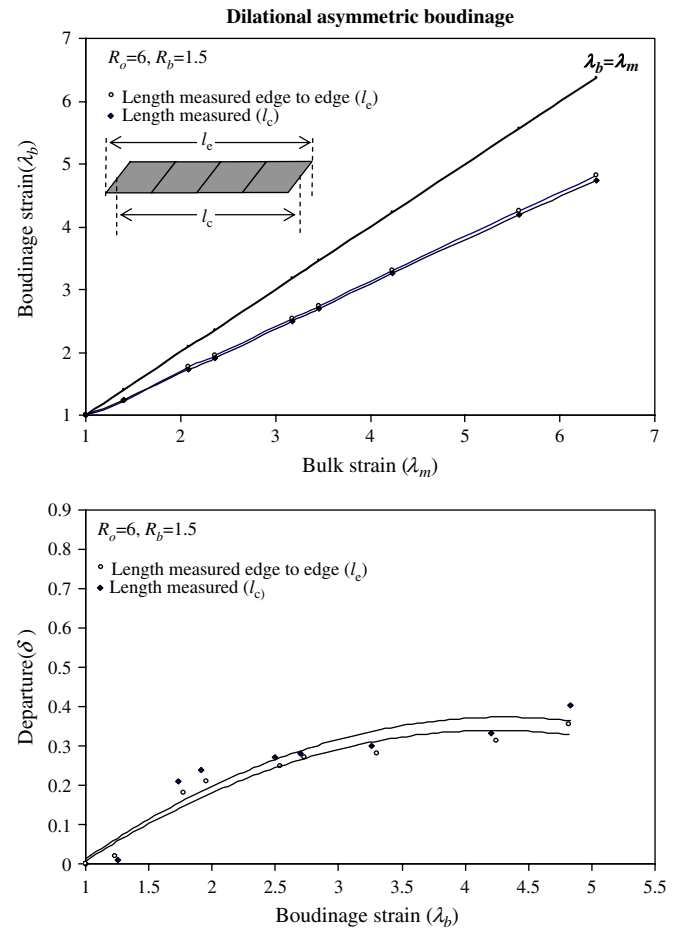

Fig. 17. λ_b versus λ_m and δ versus λ_b plots for dilational asymmetric boudinage, considering length balancing in two methods: (1) distance between two extreme edges; and (2) distance between two end points lying along the central line.

(3) For any boudin type, the difference between boudinage strain and bulk extension in simple shear is larger than that in pure shear.

(4) In simple shear antithetic slip boudinage better tracks the bulk extension compared to synthetic slip boudinage.

(5) Planar asymmetric boudins appear to be more accurate strain indicators.

Acknowledgements

References

Beach, A., 1979. The analysis of deformed belemnites. Journal of Structural Geology 1, 127−135.

Bons, P.D., Jessell, M.W., 1995. Strain analysis in deformation experiments with pattern matching or a stereoscope. Journal of Structural Geology 17, 917−921.

Burg, J.P., Harrris, L.B., 1982. Tension fractures and boudinaged oblique to the maximum extension direction: an analogy with Lüder bands. Tectonophysics 83, 347−363.

Ferguson, C.C., 1981. A strain reversal method for estimating extension from fragmented rigid inclusion. Tectonophysics 79, T43−T52.

Ferguson, C.C., 1987. Fracture and deformation histories of stretched belemnites and other rigid-brittle inclusions in tectonites. Tectonophysics 139, 255−273.

Gay, N.C., 1968. The determination of total finite strain in a rock from inclusions such as deformed pebbles. Tectonophysics 132, 297−309.

Ghosh, S.K., 1993. Structural Geology: Fundamental and Modern Developments. Pergamon Press, London.

Ghosh, S.K., Ramberg, H., 1976. Reorientation of inclusions by combination of pure shear and simple shear. Tectonophysics 34, 1−70.

Goscombe, B.D., Passchier, C.W., 2003. Asymmetric boudins as shear sense indicator-an assessment from field data. Journal of Structural Geology 25, 575−589.

Goscombe, B.D., Passchier, C.W., Hand, M., 2004. Boudinage classification: end-member boudin types and modified boudins structures. Journal of Structural Geology 26, 739−763.

Hanmer, S., Passchier, C.W., 1991. Shear-Sense Indicators: A Review. Geological Survey of Canada. Paper 90−17, 72 pp.

Hogan, J.P., Dunne, W.M., 2001. Calculation of shortening due to outcrop-scale deformation and its relation to regional deformation patterns. Journal of Structural Geology 23, 1507−1529.

Hossain, K.M., 1979. Determination of strain from stretched belemnites. Tectonophysics 60, 279−288.

Ji, S., Zhao, P., 1993. Location of tensile fracture within rigid-brittle inclusions in a ductile flowing matrix. Tectonophysics 220, 23−31.

Jordan, P., 1991. Development of asymmetric shale pull-aparts in evaporate shear zone. Journal of Structural Geology 13, 399−409.

Karmakar, S., Mandal, N., 1989. Rotation and offset of shear fracture boudins. Indian Journal of Geology 61, 41−49.

Lebit, H., Hudleston, P., Luneburg, C., 2005. Fabric, strain and structural development in three dimensions. Journal of Structural Geology 27, 1139−1142.

Lisle, R.J., 1979. Strain analysis using deformed pebbles: the influence of initial pebble shape. Tectonophysics 60, 263−277.

Lloyd, G.E., Condliffe, E., 2003. Strain reversal: a windows-based program for the calculation of strain from boudinage structures. Journal of Structural Geology 25, 1141−1145.

Lloyd, G.E., Ferguson, C.C., 1981. Boudinage structures: some new interpretations based on elastic-plastic finite-element simulation. Journal of Structural Geology 3, 117−128.

Mandal, N., Khan, D., 1991. Rotation, offset and separation of oblique fracture (rhombic) boudins: theory and experiments under layer normal compression. Journal of Structural Geology 13, 349−356.

Mandal, N., Deb, S.K., Khan, D., 1994. Evidence of nonlinear relationship between fracture spacing and layer thickness. Journal of Structural Geology 16, 1275−1281.

Mandal, N., Chakraborty, C., Samanta, S.K., 2000. Boudinage in multilayered rocks under layer-normal compression: a theoretical analysis. Journal of Structural Geology 22, 373−382.

Mandal, N., Chakraborty, C., Samanta, S.K., 2001. Controls on the failure of brittle objects hosted in a ductile matrix. Journal of Structural Geology 23, 51−66.

Mitra, S., 1976. A quantitative study of deformation mechanisms and finite strain in quartzites. Contribution to Mineralogy and Petrology 59, 203−226.

Nur, A., Ron, H., 1987. Block rotations, fault domains and crustal deformation. Annales Tectonicae 1, 40−47.

Passchier, C.W., 2001. Flanking structures. Journal of Structural Geology 23, 951−962.

Passchier, C.W., Druguet, E., 2002. Numerical modelling of asymmetric boudinage. Journal of Structural Geology 24, 1789−1803.

Ramberg, H., 1955. Natural and experimental boudinage. Journal of Geology 63, 512−526.

Ramsay, J.G., 1967. Folding and Fracturing of the Rocks. McGraw-Hill, New York and London, p. 561.

Ramsay, J.G., Huber, M.I., 1983. The Techniques of Modern Structural Geology, Vol. 1, Academic Press, London, p. 308.

Ramsay, J.G., Huber, M.I., 1987. The Techniques of Modern Structural Geology, Vol. 2, Academic Press, London, p. 700.

Ramsay, J.G., Lisle, R.J., 2000. Applications of Continuum Mechanics in Structural Geology, Vol. 3, Academic Press, London, pp. 702−1061.

Treagus, S.H., Treagus, J.E., 2001. Effects of ellipticity on strain, and implications for clast-matrix rocks. Journal of Structural Geology 23, 601−608.

Treagus, S.H., Lan, L., 2004. Deformation of square objects and boudins. Journal of Structural Geology 26, 1361−1376.